Immunity, Volume *59*

Supplemental information

Environmentally induced cell stiffening shapes metastatic site selection by tuning the immune vulnerability of cancer cells

Yassmin A. Elbanna, Maria Tello-Lafoz, Aliya Holland, Ye Zhang, Chengyuan Li, Seema Amin, Zhenghan Wang, Jun-Goo Kwak, Alexandrina Yakimov, Anastasiia Vaska, Esther Lee, Myra Dada, Samuel Vayner, Sarah M. Duquette, Young Hun Kim, Jahkwaun Budhai, Ning Fan, Erik Ladewig, Tejus A. Bale, Benjamin Y. Winer, Kenny K.H. Yu, Joan Massagué, Christina Leslie, Jungwoo Lee, Ori Barzilai, Scott R. Manalis, and Morgan Huse

Supplemental Tables

KEGG Regulation of Actin	APC, APC2, ARAF, ARHGAP35, ARHGEF1, ARHGEF12, ARHGEF4, ARHGEF6, ARHGEF7, ARPC1A, ARPC1B, ARPC2, ARPC3, ARPC4, ARPC5, ARPC5L, BAIAP2, BCAR1, BDKRB1, BDKRB2, BRAF, BRK1, CD14, CDC42, CFL1, CFL2, CHRM1, CHRM2, CHRM3, CHRM4, CHRM5, CRK, CRKL, CSK, CYFIP1, CYFIP2, DIAPH1, DIAPH2, DIAPH3, DOCK1, EGF, EGFR, ENAH, EZR, F2, F2R, FGD1, FGD3, FGF1, FGF10, FGF11, FGF12, FGF13, FGF14, FGF16, FGF17, FGF18, FGF19, FGF2, FGF20, FGF21, FGF22, FGF23, FGF3, FGF4, FGF5, FGF6, FGF7, FGF8, FGF9, FGFR1, FGFR2, FGFR3, FGFR4, FN1, GIT1, GNA12, GNA13, GNG12, GSN, HRAS, INS, INSRR, IQGAP1, IQGAP2, IQGAP3, ITGA1, ITGA10, ITGA11, ITGA2, ITGA2B, ITGA3, ITGA4, ITGA5, ITGA6, ITGA7, ITGA8, ITGA9, ITGAD, ITGAE, ITGAL, ITGAM, ITGAV, ITGAX, ITGB1, ITGB2, ITGB3, ITGB4, ITGB5, ITGB6, ITGB7, ITGB8, KRAS, LIMK1, LIMK2, MAP2K1, MAP2K2, MAPK1, MAPK3, MOS, MRAS, MSN, MYH10, MYH14, MYH9, MYL10, MYL11, MYL12A, MYL12B, MYL2, MYL5, MYL7, MYL9, MYLK, MYLK2, MYLK3, NCKAP1, NCKAP1L, NRAS, PAK1, PAK2, PAK3, PAK4, PAK5, PAK6, PDGFA, PDGFB, PDGFC, PDGFD, PDGFRA, PDGFRB, PFN1, PFN2, PFN3, PFN4, PIK3CA, PIK3CB, PIK3CD, PIK3CG, PIK3R1, PIK3R2, PIK3R3, PIK3R5, PIKFYVE, PIP4K2A, PIP4K2B, PIP4K2C, PIP5K1A, PIP5K1B, PIP5K1C, PPP1CA, PPP1CB, PPP1CC, PPP1R12A, PTK2, PXN, RAC1, RAC2, RAC3, RAF1, RDX, RHOA, ROCK1, ROCK2, RRAS, RRAS2, SCIN, SLC9A1, SOS1, SOS2, SSH1, SSH2, SSH3, TIAM1, TIAM2, TMSB4X, TMSB4XP8, TMSB4Y, VAV1, VAV2, VAV3, VCL, WAS, WASF1, WASF2, WASL

GSEA Cytoskeletal Genes	ABLIM1, ABLIM2, ABRA, ACTA1, ACTB, ACTC1, ACTG1, ACTL7A, ACTL7B, ACTN2, ACTN3, ACTR1A, ACTR1B, ACTR2, ACTR3, AIF1L, AKAP4, AKAP9, ALMS1, ALS2, AMOT, AMPH, ANLN, ANXA1, APC, APPBP2, ARHGDIA, ARHGDIB, ARHGEF2, ARL8A, ARL8B, ARPC1A, ARPC1B, ARPC2, ARPC3, ARPC4, ARPC5, ATG4A, ATG4B, ATG4C, ATG4D, AURKA, AURKC, AVIL, BASP1, BBS4, BFSP2, BIN1, BIRC5, BMF, BRCA2, BUB1, CABP1, CACNA1C, CALD1, CAPG, CAPZA1, CAPZA2, CAPZB, CASK, CASP8, CCNA1, CCNB2, CCP110, CCT3, CD2AP, CDC16, CDC20, CDC27, CDC42BPB, CDC42EP3, CDH1, CDK1, CDK5RAP2, CDSN, CENPF, CEP131, CEP250, CEP290, CEP41, CEP57, CEP63, CETN1, CETN3, CHMP1A, CKAP5, CLASP1, CLASP2, CLIC4, CLIC5, CLIP1, CLIP2, CNFN, CNN2, CNTRL, CNTROB, CORO1A, CORO1C, CROCC, CSTA, CTAG2, CTNNB1, CTTN, CTTNBP2NL, DAG1, DAPK1, DCTN1, DCTN2, DCTN3, DCTN4, DCX, DDX20, DLG4, DLGAP5, DMD, DMTN, DNAH9, DNAI1, DNAI2, DNALI1, DRD2, DSP, DYNC1I1, DYNC1LI2, DYNLL1, DYNLL2, ECPAS, EDA, EML1, EML2, ENKD1, EPB41, EPB41L2, EPB41L4B, EPB42, ESPL1, ESPN, EVPL, EZR, FARP1, FBXO5, FLNA, FLNB, FSCN1, FSCN2, FSCN3, FYB1, GABARAPL2, GAS2, GAS8, GFAP, GSN, GYPC, GYS2, HAP1, HAUS2, HDAC6, HINT1, HIP1, HSPB1, INA, INCENP, IPP, IQGAP1, IQGAP2, IVL, KALRN, KATNA1, KATNB1, KIF11, KIF15, KIF1B, KIF20B, KIF23, KIF25, KIF2C, KIF3B, KIF3C, KIF4A, KIF5A, KIF5B, KIF5C, KIFAP3, KIFC3, KLC1, KLC2, KLHL2, KLHL20, KLHL4, KNTC1, KPTN, KRT1, KRT15, KRT17, KRT18, KRT19, KRT2, KRT3, KRT31, KRT5, KRT6A, LASP1, LATS1, LATS2, LCK, LDB3, LIMA1, LLGL1, LMNB1, LORICRIN, LRPPRC, LRRFIP1, LSP1, LYST, MAP1A, MAP1B, MAP1S, MAP2, MAP3K11, MAP4, MAP7, MAPRE1, MAPT, MARCKS, MARK1, MARK4, MCF2, MEFV, MID1, MPZL2, MSN, MTSS1, MYH10, MYH6, MYH7, MYH9, MYL11, MYL2, MYL3, MYL4, MYL5, MYL6, MYL6B, MYL9, MYO18B, MYO1A, MYO1C, MYO3A, MYO6, MYO9B, MYOM1, MYOT, NARF, NDE1, NEB, NEDD9, NEFL, NEFM, NEK2, NF2, NHERF1, NIN, NPM1, NUDT21, NUMA1, PAFAH1B1, PALLD, PARVG, PCGF5, PCM1, PDLIM5, PKD2, PKHD1, PKP1, PLK1, PNN, POLB, PPL, PPP4R2, PRC1, PTK2, PTPN21, PXN, RABGAP1, RAE1, RANBP9, RNF19A, RPGRIP1L, SAC3D1, SASS6, SCEL, SEPTIN11, SEPTIN7, SEPTIN9, SHROOM1, SHROOM2, SHROOM3, SHROOM4, SIRT2, SLC30A9, SLC4A1,

	SMC3, SMTN, SORBS1, SORBS2, SPRR1A, SPRR1B, SPRR3, SPTA1, SPTAN1, SPTB, SPTBN1, SPTBN2, SPTBN4, SRCIN1, STAU1, STK38L, STOM, STOML2, SYNPO, TBCC, TBCD, TBCE, TCHP, TEX35, TGM1, THAP6, TNNC1, TNNI3, TNNT2, TOP2A, TPM1, TPM2, TPM3, TPM4, TPT1, TPX2, TRPC4, TSC1, TTK, TUBB, TUBB4B, TUBB7P, TUBD1, TUBE1, TUBG1, TUBGCP2, TUBGCP3, TUBGCP4, TUBGCP5, TUBGCP6, TWF1, UPP2, USH1G, UTRN, UXT, VASP, VILL, VIM, WAS, WASF1, WASF2, WASL, WBP2NL, WIPF1, ZW10

Table S1. Cytoskeletal gene lists. Related to Fig. 5.

Xenium add-on panel	Spp1, Mrtfb, Gzmc, Cck, Gsta4, S100a6, Pmel, Siglec15, Mpo, Thy1, Krt5, Muc5b, Slc34a2, Clec12a, Wasf2, Col3a1, Timp3, Taz, Cald1, Cnn2, Fos, Fosb, Il17b, Myl6, Pfn1, Wdr1, Plcb3, Prune2, Cfl1, Itgb1bp2, Junb, Kcnmb1, Scoc, Setd2, Slc25a4, Susd1, Ier2, Tnmd, Asb4, Car3

Table S2. Xenium add-on gene list. Related to Fig. 7.

Stiffness-related genes	Col1a1, Col1a2, Col3a1, Col5a1, Col12a1, Col14a1, Fn1, Vtn, Thbs1, Thbs2, Fbln1, Fbn1, Eln, Lox, Loxl1, Plod1, Postn, Cemip, Yap1, Wwtr1, Axl, Ajuba, Nf2, Sox9, Il11, Itgb1, Itgb4, Itga5, Itga6, Itgav, Itga11, Ptk2, Ptk2b, Src, Fyn, Vcl, Tln1, Zyx, Pxn, Parva, Parvb, Shc1, Myh9, Myh10, Myh11, Cfl1, Enah, Vasp, Cttn, Wdr1, Twf1, Rhoa, Rhoc, Rock1, Rock2, Arhgef11, Arhgef12, Diaph1, Prkaa1, Mrtfa, Mrtfb, Srf, Tagln, Actg2, Cnn1, Nr4a1, Fos, Junb, Piezo1, Piezo2, Trpv4, Kcnk2, Hif1a, Edn1, Angptl4, Vegfa, Egr1, Ptgs2, Sdc1

Table S3. Stiffness module gene list. Related to Fig. 7.

Supplemental Figures

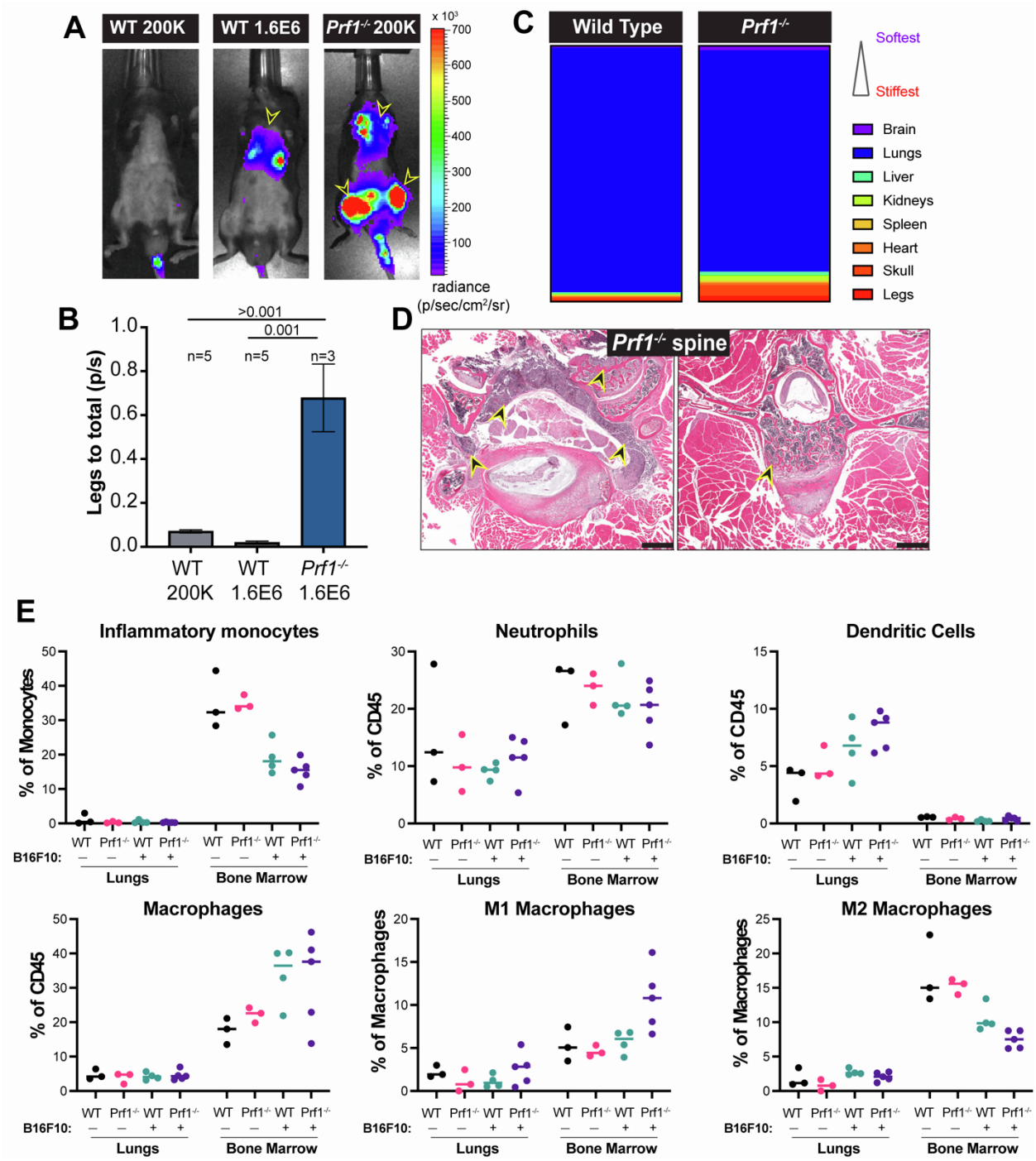

Fig. S1. Preferential suppression of bone metastasis by cytotoxic lymphocytes. Related to Fig. 2. (A-B) Wild type and *Prf1*$^{-/-}$ mice were i.v. injected with low (2×10^5) or high (1.6×10^6) doses of Luc$^+$ B16F10 cells as indicated, and the mice monitored for metastatic colonization of the lungs and bone. (A) Representative bioluminescence images of tumor-bearing wild type and *Prf1*$^{-/-}$ mice, with metastatic burden in the lungs and femurs indicated by black and yellow

arrowheads. (B) Quantification of relative femoral colonization, expressed as a ratio of bioluminescence signal in the legs to the total bioluminescence signal. Error bars denote SEM. Sample size is indicated above each bar. P-values calculated by one-way ANOVA. (C) Relative distribution of bioluminescence signal across nine organs, expressed as the fraction of total bioluminescent flux summed across all organs, from tumor-bearing wild type (n = 4) and *Prf1*$^{-/-}$ (n = 5) mice. (D) H&E images of representative B16F10 tumors found in *Prf1*$^{-/-}$ spines, with tumor cells denoted by black and yellow arrowheads. Scale bars = 500 μm. (E) Flow cytometric quantification of myeloid cell populations isolated from the lungs and bone marrow of uninjected and tumor-bearing wild type and *Prf1*$^{-/-}$ mice. Results are representative of at least two independent experiments.

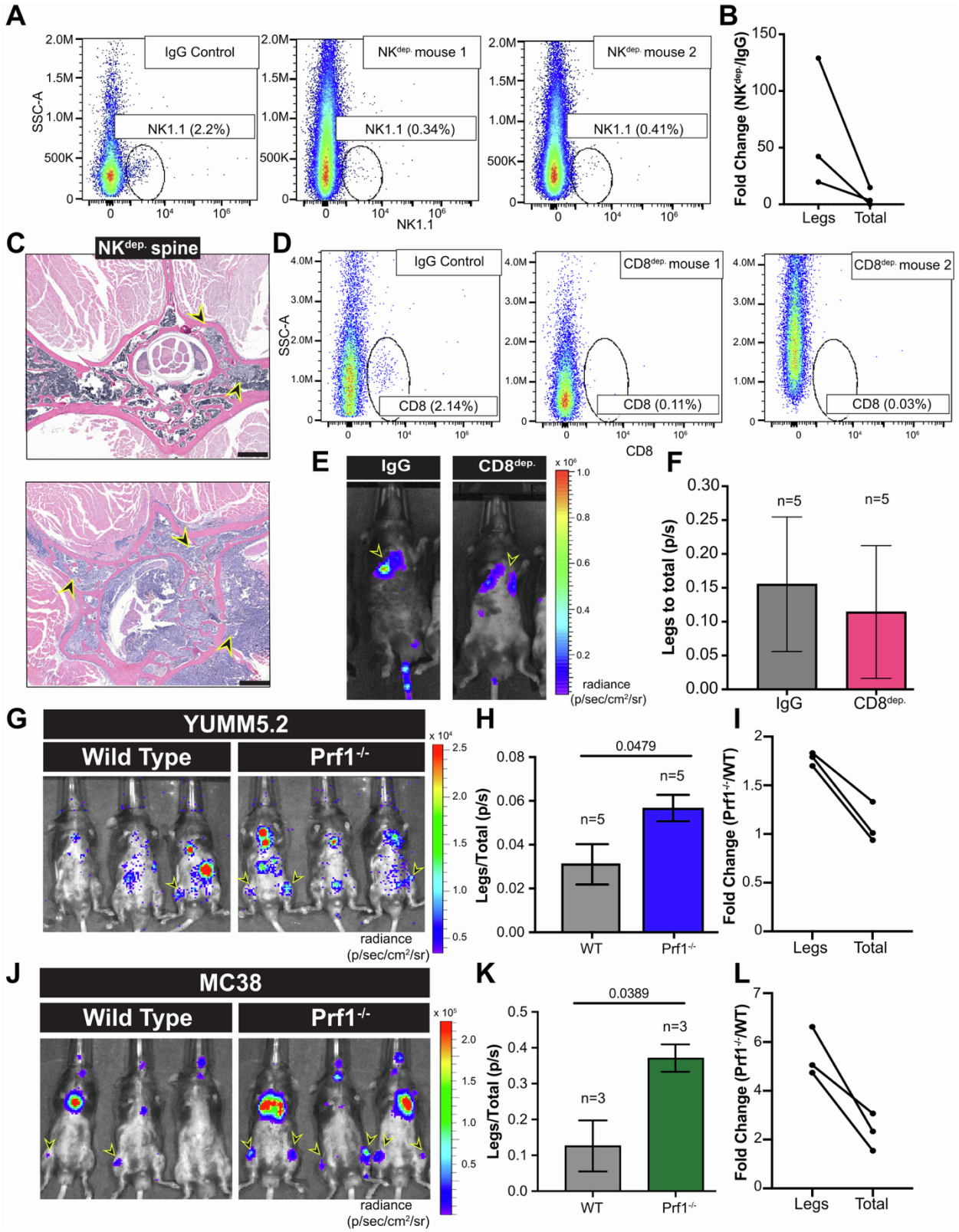

Fig. S2. Cytotoxic lymphocytes limit bone metastasis by B16F10, YUMM5.2, and MC38 cells. Related to Fig. 3. (A) Flow cytometric validation of NK cell depletion by anti-asialoGM1

antibody treatment. NK1.1 staining of blood samples from representative IgG control and NK-depleted ($NK^{dep.}$) mice is shown. (B) Mean fold change in B16F10 colonization in $NK^{dep.}$ mice relative to IgG controls, determined for total metastasis and femoral metastasis (legs). Paired values were derived from 3 independent experiments. (C) H&E images of representative metastatic tumors taken from the spines of $NK^{dep.}$ mice, with tumor cells denoted by black and yellow arrowheads. Scale bars = 500 μm. (D) Flow cytometric validation of $CD8^+$ T cell depletion by anti-CD8 antibody treatment. CD8 staining of blood samples from representative IgG control and CD8-depleted ($CD8^{dep.}$) mice are shown. (E-F) Luc^+ B16F10 cells were injected i.v. into IgG control and $CD8^{dep.}$ recipient mice, which were then monitored for metastatic colonization of the lungs and bone. (E) Representative bioluminescence images of tumor-bearing IgG control and $CD8^{dep.}$ mice, with metastatic burden in the lungs indicated by black and yellow arrowheads. (F) Quantification of relative femoral colonization, expressed as a ratio of bioluminescence signal in the legs to the total bioluminescence signal. Error bars denote SEM. Sample size is indicated above each bar. (G-L) Luc^+ YUMM5.2 (G-I) and MC38 (J-L) cells were injected i.c. into wild type and *Prf1*$^{-/-}$ recipient mice, which were then monitored for metastatic colonization of the lungs and bone. (G and J) Representative bioluminescence images of tumor-bearing wild type and *Prf1*$^{-/-}$ mice, with metastatic YUMM5.2 (G) and MC38 (J) burden in the lungs and femurs indicated by black and yellow arrowheads. (H and K) Quantification of relative femoral colonization, expressed as a ratio of YUMM5.2 (H) and MC38 (K) bioluminescence signal in the legs to the total bioluminescence signal. Error bars denote standard error of the mean (SEM). Sample size is indicated above each bar. P-values calculated by unpaired Student's t-test. (I and L) Mean fold changes in YUMM5.2 (I) and MC38 (L) colonization in *Prf1*$^{-/-}$ mice relative to wild type controls, determined for total metastasis and femoral metastasis (legs). Results are representative of at least two independent experiments.

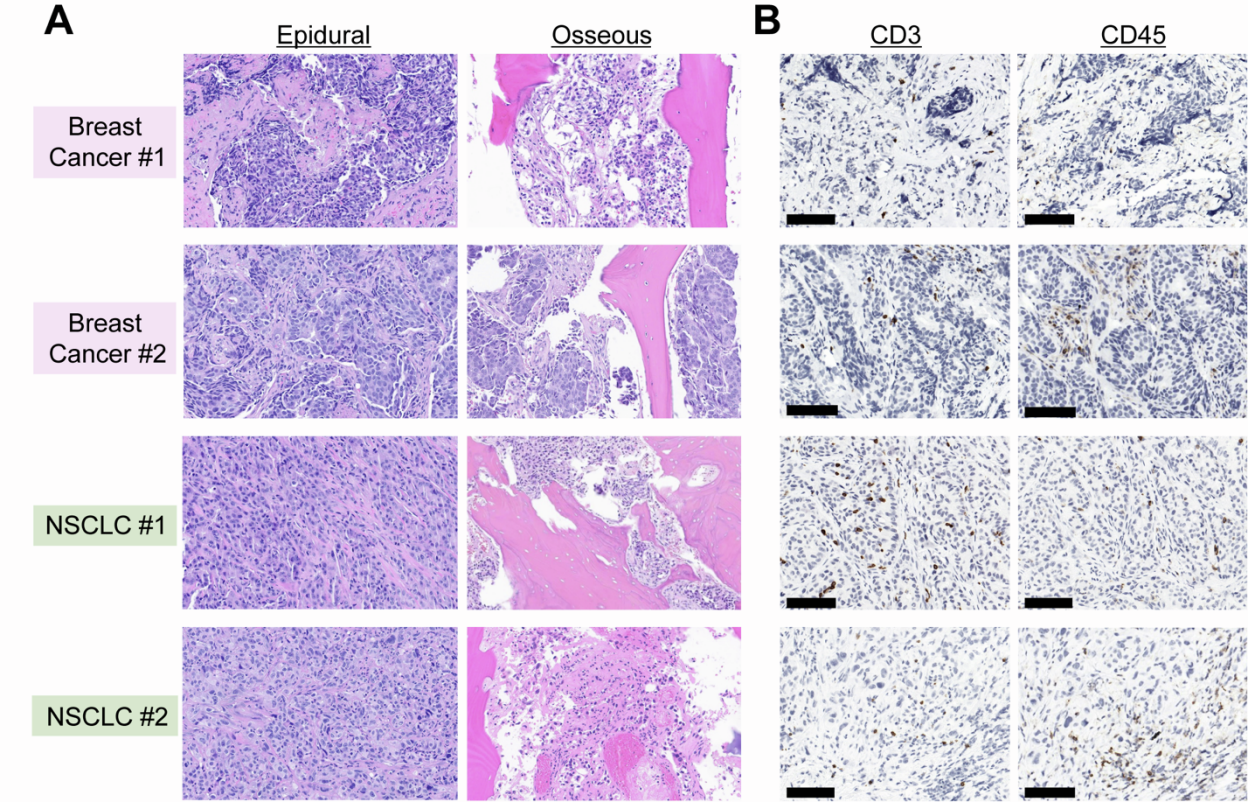

Fig. S3. Histological analyses of patient spinal metastases. Related to Fig. 4. (A) H&E staining of representative sections from epidural and osseous regions of the indicated tumors. (B) IHC staining of CD3 and CD45 in representative epidural sections of the indicated tumors. Scale bars = 100 μm.

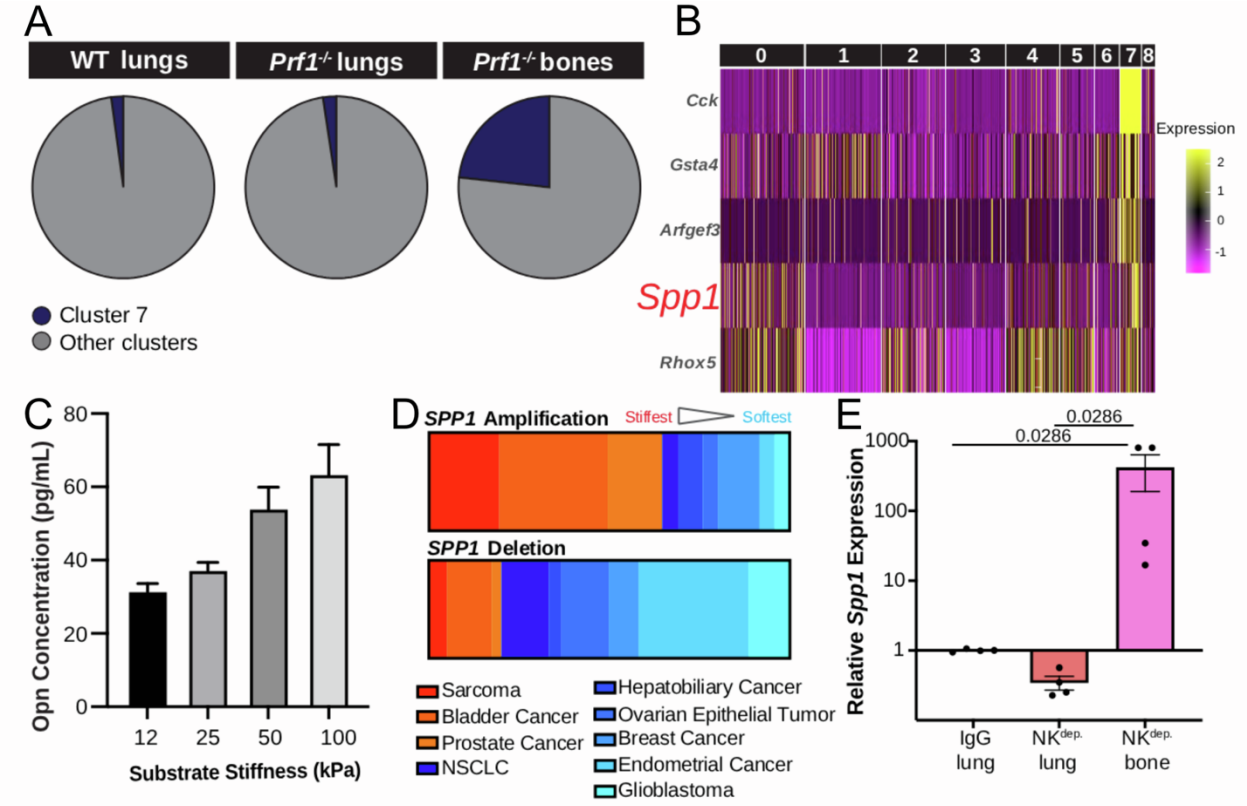

Fig. S4. Osteopontin is a feature of bone metastasis. Related to Fig. 5. (A) GFP^{+} B16F10 cells were i.v. injected into wild type or *Prf1*$^{-/-}$ mice, and after 2 weeks, MTCs from the resulting metastases in the lungs of wild type mice and the lungs and bones of *Prf1*$^{-/-}$ mice were extracted and subjected to scRNA-seq. Pie charts showing the proportion of cluster 7 cells (see Fig. 5A) in each MTC sample. (B) Heatmap showing the top 5 differentially expressed genes in cluster 7. (C) Osteopontin (Opn) release from B16F10 cells cultured overnight on hydrogel substrates of the indicated stiffnesses was quantified by ELISA. Error bars indicate SEM, determined from technical triplicates. (D) The relative frequency of *SPP1* amplification and deletion in human tumors, determined using TCGA data. Tumors are organized according to the rigidity of their parent tissue. (E) qRT-PCR analysis of *Spp1* expression in MTCs extracted from the indicated organs in IgG-treated versus NK$^{dep.}$ tumor-bearing mice. Error bars denote SEM. P-values calculated by one-sample Wilcoxon test. All results are representative of at least two independent experiments.

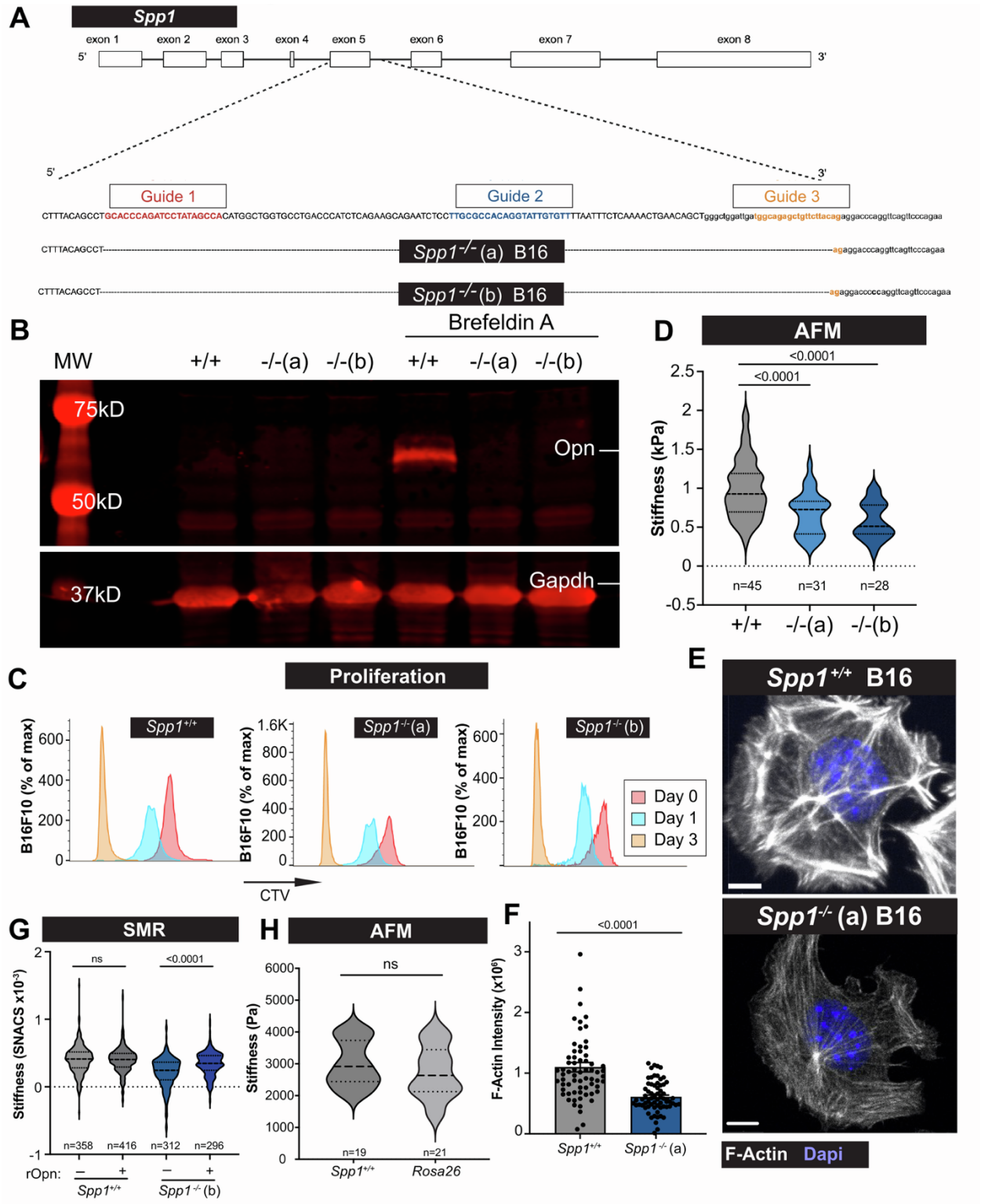

Fig. S5. Osteopontin regulates stiffness but does not affect proliferation. Related to Fig. 5. (A) Schematic diagram of the CRISPR/Cas9 multi-guide approach used to knock out *Spp1* in B16F10 cells. The exon configuration of the gene is shown above and the targeted locus below,

along with the 134 bp and 132 bp deletions induced in *Spp1*$^{-/-}$(a) and *Spp1*$^{-/-}$(b), respectively. (B) Immunoblot analysis of osteopontin expression in *Spp1*$^{+/+}$ and *Spp1*$^{-/-}$ B16F10 cell lines. Samples were treated with Brefeldin A as indicated to suppress the release of secreted proteins. Gapdh served as a loading control. (C) The indicated B16F10 cell lines were stained with cell trace violet (CTV), and their proliferation assessed by dye dilution. Representative flow cytometric measurements of CTV fluorescence after 0, 1, and 3 days of culture are shown. (D) The indicated *Spp1*$^{-/-}$ B16F10 cell lines, along with nontargeting *Spp1*$^{+/+}$ B16F10 control cells, were subjected to AFM. (E-F) Phalloidin staining of the indicated *Spp1*$^{-/-}$ and *Spp1*$^{+/+}$ B16F10 cells. (E) Images of representative cells, with nuclei visualized using DAPI. Scale bars = 8 μm. (F) Quantification of F-actin intensity, with error bars indicating SEM. (G) The indicated B16F10 cell lines were treated with purified osteopontin protein overnight and then subjected to SMR analysis. (H) AFM stiffness measurements of *Spp1*$^{+/+}$ B16F10 cells and *Rosa26* targeted “safe harbor” B16F10 controls. In D, G, and H, violins encompass the entire data distribution, with dashed lines denoting the median and dotted lines indicating the upper and lower quartiles. Sample size is indicated below each violin. P-values calculated by one way ANOVA (D and G) and by unpaired t-test (F and H).

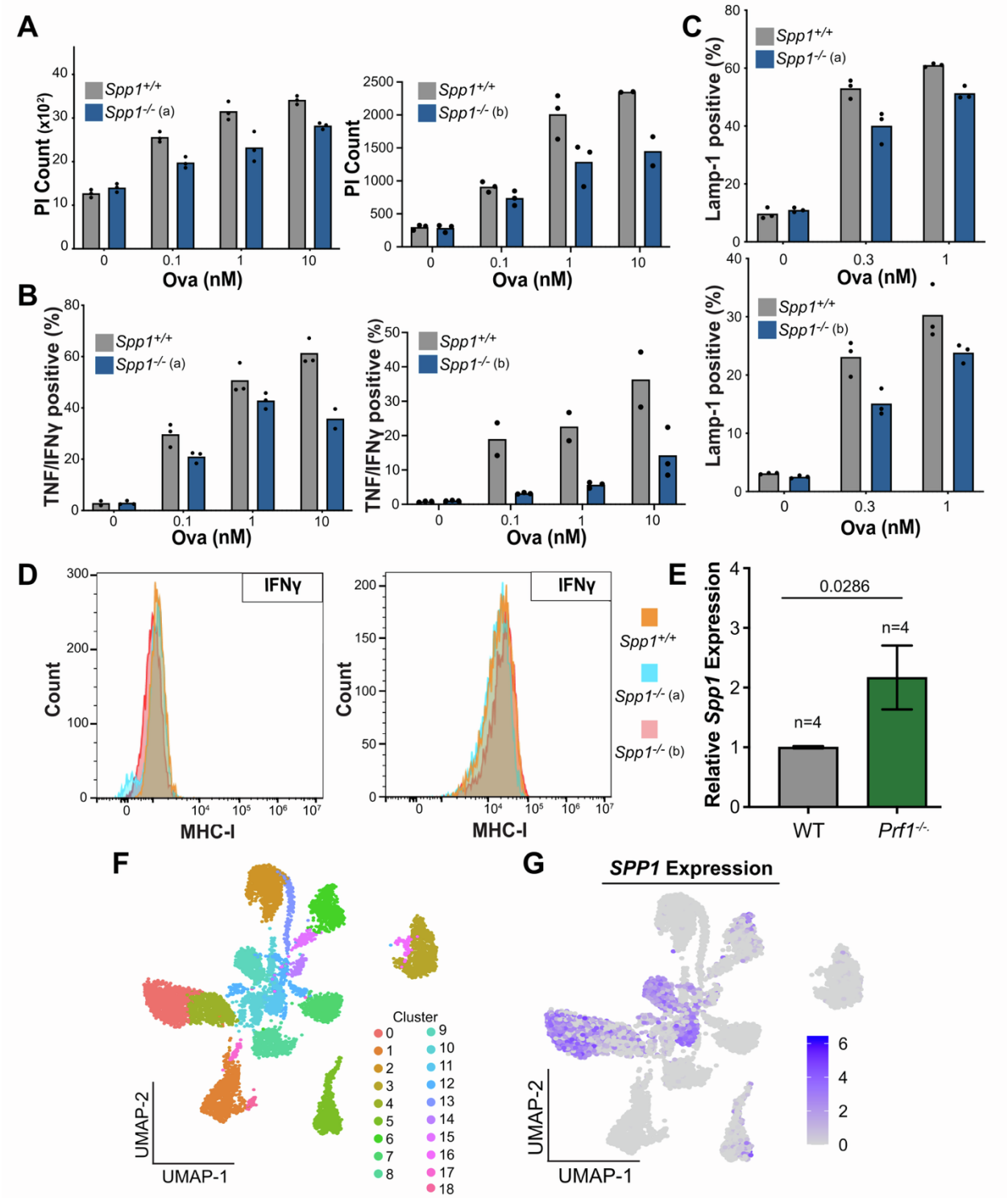

Fig. S6. Osteopontin sensitizes B16F10 cells to cytotoxic lymphocytes. Related to Fig. 5. (A-C) The indicated B16F10 cells were loaded with increasing amounts of OVA and then mixed with OT-1 CTLs. (A) Target cell killing, measured by PI influx after 5 h. (B) CTL cytokine production, measured by intracellular staining for TNF and IFNγ, after 5 h. (C) Degranulation,

measured by surface exposure of Lamp1, after 90 min. (D) Representative histograms showing MHC-I expression by the indicated B16F10 cells lines, determined in the absence (left) or presence (right) of 20 ng/mL IFNγ, which promotes MHC-I upregulation. (E) qRT-PCR analysis of *Spp1* expression in MC38 MTCs extracted from the bones of wild type and *Prf1*$^{-/-}$ tumor-bearing mice. Error bars denote SEM. P-value calculated by Mann-Whitney test. Results in A-E are representative of at least two independent experiments. (F-G) scRNA-seq analysis of cytoskeletal gene expression in a published cohort of melanoma patients[59]. (F) UMAP visualization of the transcriptomic data, colored by Seurat cluster. (G) Feature plot showing *SPP1* expression across the entire data set.

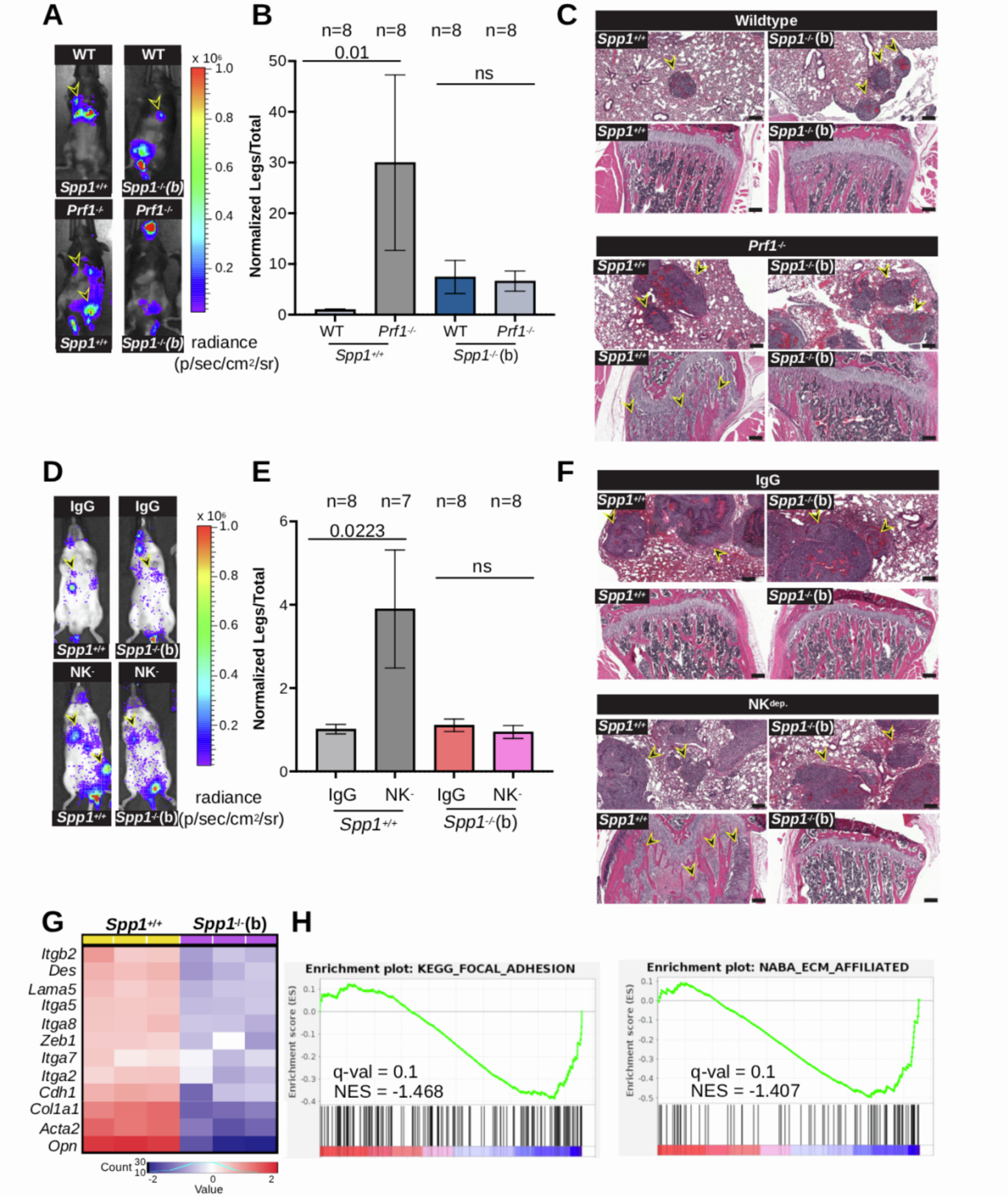

Fig. S7. Osteopontin is required for bone colonization. Related to Fig. 6. (A-C) Luc^{+} *Spp1*$^{+/+}$ or *Spp1*$^{-/-}$(b) B16F10 cells were injected i.v. into wild type and *Prf1*$^{-/-}$ mice, which were then monitored for metastatic colonization of the lungs and bone. (A) Representative bioluminescence images of tumor-bearing wild type and *Prf1*$^{-/-}$ mice injected with the indicated B16F10 lines, with

metastatic burden in the lungs and femurs indicated by black and yellow arrowheads. (B) Quantification of relative femoral colonization, expressed as a normalized ratio of bioluminescence signal in the legs to the total bioluminescence signal. (C) Representative H&E sections highlighting the absence of femoral colonization in *Prf1*$^{-/-}$ mice injected with *Spp1*$^{-/-}$(b) B16F10 cells. Lung metastases and *Spp1*$^{+/+}$ B16F10 metastases in *Prf1*$^{-/-}$ bone are indicated by black and yellow arrowheads. Scale bars = 200 μm. (D-F) Luc^{+} *Spp1*$^{+/+}$ or *Spp1*$^{-/-}$(b) B16F10 cells were injected i.v. into IgG control and NK$^{dep.}$ recipient mice, which were then monitored for metastatic colonization of the lungs and bone. (D) Representative bioluminescence images of tumor-bearing IgG control and NK$^{dep.}$ mice injected with the indicated B16F10 lines, with metastatic burden in the lungs and femurs indicated by black and yellow arrowheads. (E) Quantification of relative femoral colonization, expressed as a normalized ratio of bioluminescence signal in the legs to the total bioluminescence signal. (F) Representative H&E sections highlighting the absence of femoral colonization in NK$^{dep.}$ mice injected with *Spp1*$^{-/-}$(b) B16F10 cells. Lung metastases and *Spp1*$^{+/+}$ B16 metastases in NK$^{dep.}$ bone are indicated by black and yellow arrowheads. Scale bars = 200 μm. In B and E, Legs/Total ratios were pooled from two independent experiments. Error bars denote SEM, sample size is indicated above each bar, and P-values were calculated by one-way ANOVA. (G-H) *Spp1*$^{+/+}$ and *Spp1*$^{-/-}$(b) B16F10 cells were subjected to comparative bulk RNA-seq. (G) Heat map showing downregulation of selected ECM, adhesion, and cytoskeleton-related genes in *Spp1*$^{-/-}$(b) cells. (H) Gene Set Enrichment Analysis (GSEA) showing downregulation of genes related to focal adhesions (left) and ECM (right) in *Spp1*$^{-/-}$(b) cells. NES = normalized enrichment score.

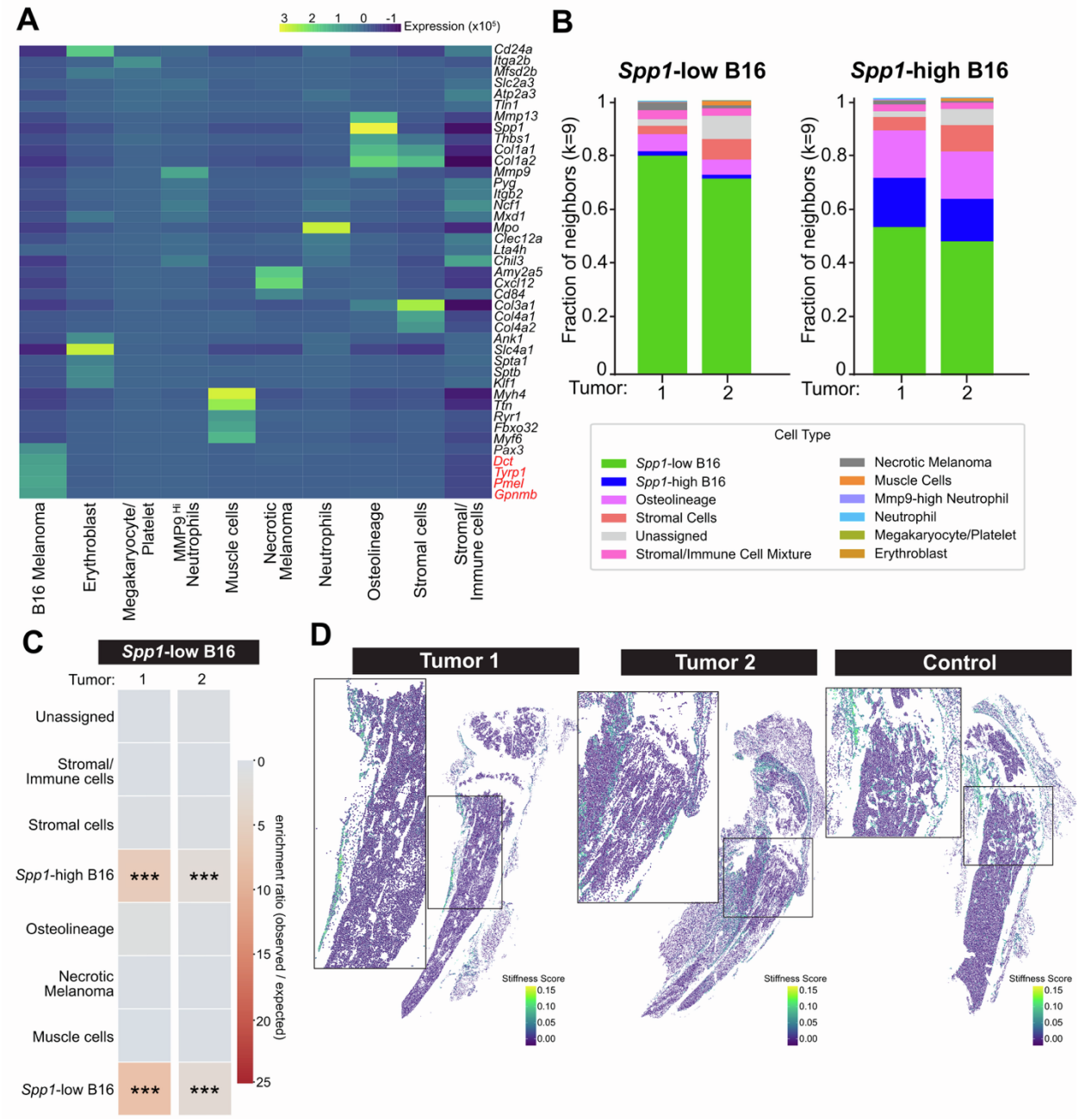

Fig. S8. Cancer cell-derived osteopontin promotes cell stiffness and colocalization with osteolineage cells *in vivo*. Related to Fig. 7. Xenium spatial transcriptomic analysis was performed on tumor-bearing and healthy *Prf1*$^{-/-}$ bones. (A) Differential gene expression heat map of segmented cells, showing cell identities and critical differentially expressed genes. Characteristic melanoma genes have been highlighted in red. (B) Nearest neighbor analysis of *Spp1*-low (left) and *Spp1*-high (right) melanoma cells, expressed as fractions of the total for each tumor sample. (C) The spatial proximity of each cell type to *Spp1*-low melanoma cells, expressed as a ratio of observed to expected distance. *** denotes P < 0.001, calculated by permutation

test. (D) A stiffness score was calculated for each cell based on its expression of 79 stiffness related genes (Table S3). These scores were then mapped onto tumor and healthy control sections. Insets show boxed regions at higher magnification.